Phys. Med. Biol. **40** (1995) 1983–1993. Printed in the UK

# Determination of optical properties and blood oxygenation in tissue using continuous NIR light

Hanli Liu†, David A Boas‡, Yutao Zhang†, Arjun G Yodh‡ and Britton Chance†

† Department of Biochemistry and Biophysics, University of Pennsylvania, Philadelphia, PA 19104, USA

‡ Department of Physics, University of Pennsylvania, Philadelphia, PA 19104, USA

Received 24 March 1995, in final form 1 August 1995

**Abstract.** In this article, we introduce a simple method to characterize optical properties and blood oxygenation in tissue using spatially resolved, steady-state reflectance. The method considers multiple source–detector separations larger than 2 cm, i.e. 20 times the optical mean free path in tissue, and makes an approximation to linearize the relationship between the separation and reflectance. Simulation results show that errors of the algorithm due to the approximation are less than 10%. Using a calibration sample, we calculate from the slope and intercept the absorption and reduced scattering coefficients, $\mu_a$ and $\mu_s'$, of a tissue-like solution, and experimental results confirm the usefulness of the method for quantitation of haemoglobin saturation in tissue.

Knowledge of tissue optical properties in the near infrared (NIR) range is of great importance in medical applications using light. For example, variation of light absorption in tissue enables one to monitor changes in blood oxygenation and concentrations of oxygenated and deoxygenated haemoglobin (Chance *et al* 1988a, b, Cope and Delpy 1988). In recent years, NIR light in forms of pulsed, amplitude-modulated, and steady-state has been used non-invasively to study optical properties and haemoglobin saturation in tissue (Delpy *et al* 1988, Tamura *et al* 1990, Sevick *et al* 1991, Farrell *et al* 1992a, b, Fantini *et al* 1995). Among these techniques, the continuous wave radiation method is the simplest. Many researchers have made great efforts and progress in using steady-state NIR light to monitor haemoglobin saturation and its changes in living organs. Such efforts include measurements of optical densities (OD) due to changes in cerebral oxygenation (Jöbsis 1977, Ferrari *et al* 1986, Thorniley *et al* 1990, Bank and Chance 1994). However, this method gives only a relative change in blood saturation and concentration. Another example is the introduction of a differential pathlength factor, DPF, for compensating the pathlength increase due to multiple light scattering in tissue (Delpy *et al* 1988, Cope *et al* 1991). Unfortunately, DPF is empirical and may vary with different subjects (Ferrari *et al* 1993). A recent study reports the use of water absorption as a comparison signal to quantify deoxy-haemoglobin concentration, but here one must combine this method with another technique to obtain an absolute value of haemoglobin saturation (Matcher and Cooper 1994).

Recently, Farrell *et al* (1992a, b) employed spatially resolved, steady-state reflectance to determine tissue absorption and scattering coefficients ($\mu_a$ and $\mu_s'$), thus providing a non-invasive means to quantify blood oxygenation in tissue with NIR continuous wave radiation. This technique requires several measurements starting from small source–detector separations, ~1–5 mm, and utilizes a complex fitting routine and powerful computer (Farrell

0031-9155/95/111983+11$19.50  

*et al* 1992b). In order to have good spatial resolution when source–detector separations are 5 mm or smaller, one has to limit the size of the fibres or detectors. In turn, this results in smaller signal-to-noise ratios when the source–detector separations increase to 3–4 cm and more. Such large separations are necessary for determination of haemoglobin saturation deep in tissues.

In this article, we introduce a simple method to measure and analyse spatially resolved, steady-state reflectance data to characterize optical properties and blood oxygenation in bulk tissue. The method considers source–detector separations larger than 2 cm and makes an approximation to linearize the relationship between the reflectance and separation. We present an error analysis by comparing the simplified algorithm with the exact solution and then show experimental results analysed with this method.

According to diffusion theory, the spatial dependence of the diffuse reflectance, $R(\rho)$, of continuous light remitted from a semi-infinite scattering medium at a separation of $\rho$ from the source is (Farrell *et al* 1992a, b)

$$R(\rho) = \frac{I_0}{4\pi\mu_t'}\left[\left(\mu_{eff}+\frac{1}{r_1}\right)\frac{e^{-\mu_{eff}r_1}}{r_1^2}+\left(\tfrac{4}{3}A+1\right)\left(\mu_{eff}+\frac{1}{r_2}\right)\frac{e^{-\mu_{eff}r_2}}{r_2^2}\right] \quad (1)$$

where $r_1 = \sqrt{(1/\mu_t')^2+\rho^2}$, $r_2 = \sqrt{\left[\left(\frac{4}{3}A+1\right)/\mu_t'\right]^2+\rho^2}$, $\mu_t' = \mu_a + \mu_s'$, $\mu_{eff} = \sqrt{3\mu_a(\mu_a+\mu_s')}$, $I_0$ is the initial light source intensity, and $A$ is an internal specular reflection parameter, depending only on the relative refractive index of the tissue and surrounding medium. For a source–detector separation, $\rho$, much larger than $l_t = 1/\mu_t'$, where $l_t$ is the photon transport mean free path, we can have $r_1 \approx r_2 \approx \rho$. For typical biological samples with $\mu_a = 0.05$–$0.5$ cm$^{-1}$ and $\mu_s' = 10$–$20$ cm$^{-1}$, the mean free path, $l_t$, is in the range of 0.5–1.0 mm. Then, at $\rho > 2$ cm $\approx 20$–$40\ l_t$, equation (1) can be approximated as

$$R_{app}(\rho) = \frac{1}{a\mu_t'}\left(\mu_{eff}+\frac{1}{\rho}\right)\frac{e^{-\mu_{eff}\rho}}{\rho^2} \quad (2)$$

where $a = 2\pi/\left[I_0(1+\frac{2}{3}A)\right]$ is independent of $\rho$. It follows that

$$\log[\rho^2 R_{app}(\rho)] = -\frac{\mu_{eff}}{2.3}\rho - \log(a\mu_t') + \log\left(\mu_{eff}+\frac{1}{\rho}\right). \quad (3)$$

The last term in equation (3) is non-linear and can be approximated by $\log[\mu_{eff}+(1/\rho_0)]$, where $\rho_0$ is the middle point of the chosen minimum and maximum source–detector separations in the measurement. In this way, we obtain a linear dependence of $\log[\rho^2 R_{app}(\rho)]$ on the source–detector separation $\rho$ as

$$\log[\rho^2 R_{app}(\rho,\rho_0)] = -\frac{\mu_{eff}}{2.3}\rho - \log(a\mu_t') + \log\left(\mu_{eff}+\frac{1}{\rho_0}\right). \quad (4)$$

Figure 1 shows the errors of the approximated solution, equation (4), with respect to the exact solution, equation (1), by calculating Error $= \left\{\log[\rho^2 R(\rho)] - \log[\rho^2 R_{app}(\rho,\rho_0)]\right\} / \left\{\log[\rho^2 R(\rho)]\right\} * 100\%$. This analysis indicates that equation (4) is accurate enough to replace equation (1) for data reduction to obtain $\mu_{eff}$ and $\mu_t'$, and thus $\mu_a$ and $\mu_s'$, when input–output separations are 10–20 times larger than the optical mean free path.

Equation (4) indicates that the slope of $\log[\rho^2 R_{app}(\rho,\rho_0)]$ versus the source–detector separation, $\rho$, gives $\mu_{eff}$, and thus to the product of $\mu_a$ and $\mu_t'$. It has been shown (Peters

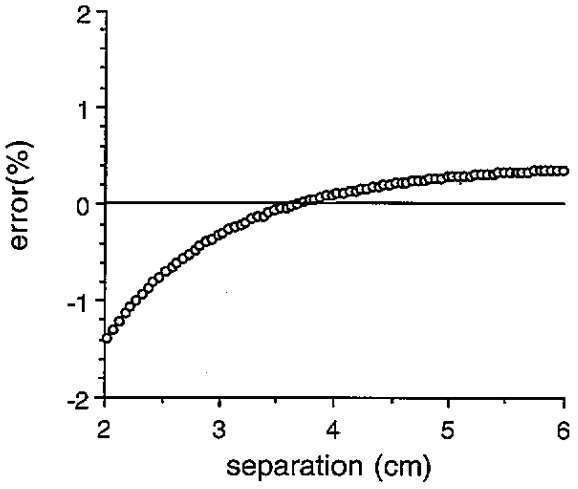


**Figure 1.** Simulated relationship of source–detector separation and errors of the approximated solution, equation (4), with respect to the exact equation, equation (1). Some parameters used are $\mu_a = 0.1$ cm$^{-1}$, $\mu_s' = 10$ cm$^{-1}$, normalized initial light intensity $I_0 = 1$, and matched refractive index condition $A = 1$. The constant, $\rho_0$, used in the approximated equation is 4 cm for $\rho_{min} = 2$ cm and $\rho_{max} = 6$ cm.

*et al* 1990, Parsa *et al* 1989) that in the wavelength range of 600–900 nm, the reduced scattering coefficients, $\mu_s'$, vary slowly with wavelength, i.e. $\mu_s'(\lambda_1) \approx \mu_s'(\lambda_2)$. Then, for dual wavelengths, it follows that

$$\frac{\text{slope}(\lambda_1)}{\text{slope}(\lambda_2)} = \frac{\mu_{\text{eff}}(\lambda_1)}{\mu_{\text{eff}}(\lambda_2)} = \frac{\sqrt{3\mu_a(\lambda_1)\mu_t'(\lambda_1)}}{\sqrt{3\mu_a(\lambda_2)\mu_t'(\lambda_2)}} \approx \sqrt{\frac{\mu_a(\lambda_1)}{\mu_a(\lambda_2)}}. \tag{5}$$

It is known that the haemoglobin saturation in tissue can be calculated by using either the absolute $\mu_a$ values at two wavelengths or the ratio of these two $\mu_a$ values (Sevick *et al* 1991, Liu *et al* 1995). Equation (5) suggests that determination of the slopes from two-wavelength, steady-state reflectance measurements can result directly in the blood oxygenation regardless of the initial light intensity. The accuracy of equation (5) is affected mainly by the assumption of $\sqrt{[\mu_s'(\lambda_1)]/[\mu_s'(\lambda_2)]} = 1$. Based on

$$\sqrt{\frac{\mu_s'(\lambda_1)}{\mu_s'(\lambda_2)}} = \sqrt{1 + \frac{\mu_s'(\lambda_1) - \mu_s'(\lambda_2)}{\mu_s'(\lambda_2)}} \simeq 1 + \frac{1}{2}\frac{\mu_s'(\lambda_1) - \mu_s'(\lambda_2)}{\mu_s'(\lambda_2)}$$

the error of equation (5) is $\frac{1}{2}[\mu_s'(\lambda_1) - \mu_s'(\lambda_2)]/[\mu_s'(\lambda_2)]$, which is about less than 10% in most tissue cases if $\lambda_1$ and $\lambda_2$ are not more than 150 nm apart (Peters *et al* 1990, Parsa *et al* 1989).

In order to determine $\mu_a$ and $\mu_s'$ from the slope and intercept of equation (4), one needs to know the factor '$a$', which is related to the initial light intensity, $I_0$, and internal specular reflection parameter, $A$. In practice, however, it is not convenient to measure an accurate value of '$a$' in each experiment. An alternative way is to utilize a calibration sample, which has known optical properties similar to tissues. We can define an optical density such that

$$\text{OD} = \log\left[\frac{R_{\text{app0}}(\rho, \rho_0)}{R_{\text{app}}(\rho, \rho_0)}\right] = \frac{\mu_{\text{eff}} - \mu_{\text{eff}}(\text{cal})}{2.3}\rho + \log\left[\frac{\mu_t'}{\mu_t'(\text{cal})}\right] + \log\left[\frac{\mu_{\text{eff}}(\text{cal}) + (1/\rho_0)}{\mu_{\text{eff}} + (1/\rho_0)}\right] \tag{6}$$

where $R_{app0}(\rho, \rho_0)$ and $R_{app}(\rho, \rho_0)$ are the reflectance obtained from the calibration and unknown sample, respectively. Equation (6) shows a linear relationship between OD and the source–detector separation, $\rho$. Given the optical properties of the calibration sample and maximum and minimum source–detector separations, the slope and intercept of this equation depend only on $\mu_a$ and $\mu_s'$ of the unknown sample. Therefore, determination of the slope and intercept of OD versus separation allows one to characterize the absorption and scattering properties or changes of an unknown sample with respect to the calibration sample. If the unknown sample has a larger value of $\mu_{eff}$ than the calibration sample, the slope is positive; otherwise, the unknown sample with a smaller $\mu_{eff}$ will give a negative slope. A larger difference in $\mu_{eff}$ between the two samples leads to a steeper slope. Based on equation (6), figures 2(a) and (b) simulate the dependence of the slope and intercept of OD on the optical properties of the unknown sample. In both cases, the $\mu_a$ and $\mu_s'$ for the calibration sample are 0.1 $cm^{-1}$ and 10 $cm^{-1}$, respectively.

In order to verify the accuracy of this approximated, linear-fitting algorithm, we perform an error analysis using the following procedures: (i) a series of input optical parameters, $\mu_a$ and $\mu_s'$, were chosen for a sample under study, and corresponding spatially resolved reflectance, $R(\rho)$, was simulated using the exact analytical solutions. (ii) After fixing a set of $\mu_a$(cal) and $\mu_s'$(cal) for the calibration sample, we obtained a simulated relationship of OD versus $\rho$ by calculating $\log[R_{cal}(\rho)/R(\rho)]$. (iii) A linear least-squares fitting routine was used to determine the slope and intercept with $\rho$ varying from 2–5 cm and 3–6 cm, and the output values of $\mu_{eff}$ and $\mu_t'$, and thus $\mu_a$ and $\mu_s'$, were computed. (iv) The comparison was made between the output optical parameters and the initial input values, and the errors for $\mu_a$ and $\mu_s'$ were defined as $E(\mu_a) = \{[\mu_a(\text{input}) - \mu_a(\text{output})]/[\mu_a(\text{input})]\} \times 100\%$ and $E(\mu_s') = \{[\mu_s'(\text{input}) - \mu_s'(\text{output})]/[\mu_s'(\text{input})]\} \times 100\%$, respectively. Figure 3(a) shows the output $\mu_a$ and $\mu_s'$ errors as a function of input $\mu_s'$ values varying from 5–20 $cm^{-1}$ for two sets of source–detector separations of 2–5 cm and 3–6 cm. Figure 3(b) gives the dependence of the output $\mu_a$ and $\mu_s'$ errors on the input $\mu_a$ values. These two figures indicate that the errors of the approximation in most cases are within 10%. The error can be minimized if the calibration sample is chosen to have optical properties similar to the unknown sample. This indicates a potential use of the method to detect small changes in optical properties of the sample.

Besides theoretical derivation and error analysis, experimental confirmation is conducted to show the effectiveness of the method. The schematic electrical set-up is given in figure 4, showing three lightbulbs located at 3, 5, and 7 cm away from the silicon diode detector. The three bulbs flash in sequence, and their intensities are adjusted by the corresponding variable resistors for compensating the distance difference. The detector is covered by 850 nm and/or 760 nm filters; the three time-shared, detected signals are sent to the amplifier and then to the recorder. The sources and detector are mounted on a flexible tape, which is attached outside of a cylindrical, 1 L container containing the liquid sample.

In ink–Intralipid experiments, the unknown sample was made of 0.5% Intralipid solution (20% IV Fat Emulsion, Kabi Pharmacia Inc., Clayton, NC, USA) with titration of an equal amount of ink for each measurement; the initial solution without ink was used as the calibration sample. Intralipid solution itself has no extra absorption in addition to the water absorption. More detailed information on the Intralipid optical parameters and their association with real-tissue parameters can be found elsewhere (Flock *et al* 1992, van Staveren *et al* 1991). In principle, the addition of ink into the solution changes mainly the absorption coefficient of the sample solution without disturbing its scattering property. In blood–yeast experiments, the 1 L liquid sample was made of 0.6% Intralipid mixed with 1.54 mg baker's yeast powder and 2% rat blood. The initial sample solution was in a

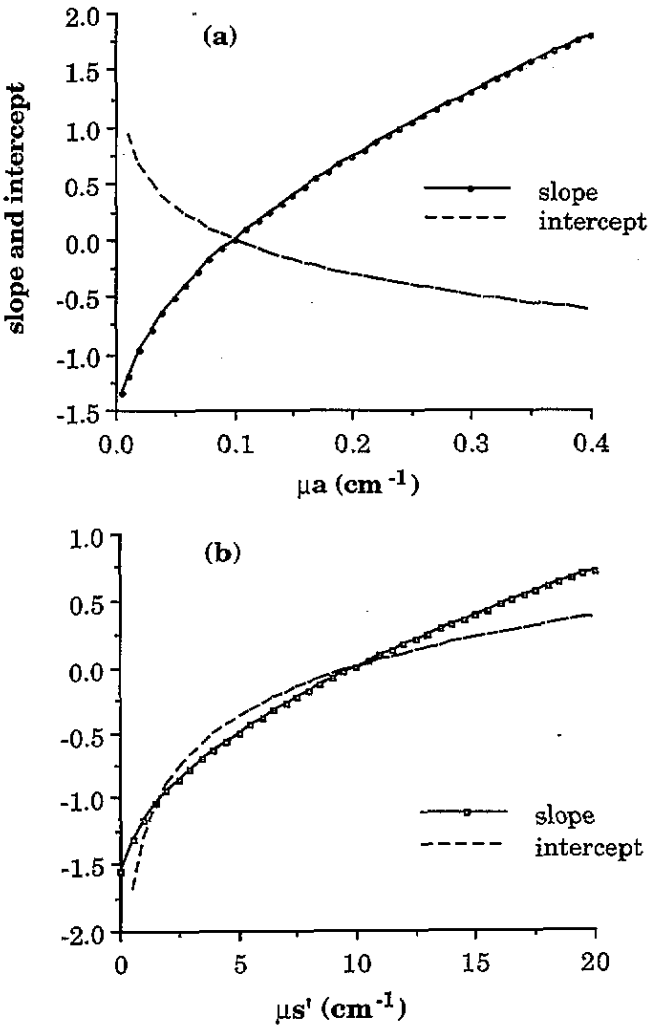


**Figure 2.** The slope (solid curves) and intercept (dashed curves) of OD as a function of the (a) absorption and (b) reduced scattering coefficients of the unknown sample. In case (a), $\mu_s'$ of the sample under study remains 10 $cm^{-1}$, whereas in case (b), $\mu_a$ of the sample under study is unchanged and equals 0.1 $cm^{-1}$. The parameters for the calibration sample are $\mu_a(cal) = 0.1$ $cm^{-1}$ and $\mu_s'(cal) = 10$ $cm^{-1}$.

deoxygenated state due to the oxygen consumption of the yeast, and this initial solution was used as the calibration sample. By bubbling and then discontinuing oxygen gas in the solution, the blood–yeast sample was varied between oxygenated and deoxygenated states. Accordingly, the absorption coefficients of the solution will change depending on the specific oxygenated states.

Figure 5 is a set of $\mu_a$ and $\mu_s'$ results based on the slope and intercept of ink–Intralipid OD measurements at 760 nm and 850 nm. Figure 5(a) shows a linear relationship between the $\mu_a$ values determined with a spectrophotometer and with the OD method at 760 nm, while figure 5(b) illustrates the independence of $\mu_s'$ values on the $\mu_a$ values of the solution at the two wavelengths. The average $\mu_s'$ value is 4.87 $cm^{-1}$, corresponding to an optical

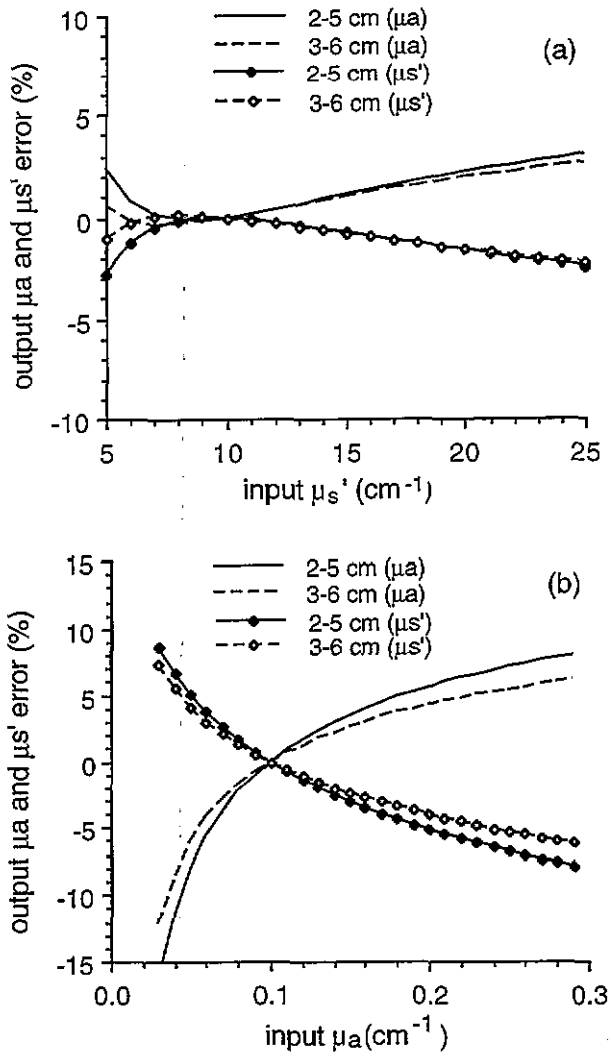


**Figure 3.** Simulated relationship between the output $\mu_a$ and $\mu_s'$ errors and the input parameters at source–detector separations of 2 to 5 cm (solid lines) and 3 to 6 cm (dashed lines). In case (a), $\mu_s'$ of the sample under study varies from 5 to 25 $cm^{-1}$, whereas $\mu_a$ of the sample under study is fixed at 0.1 $cm^{-1}$. In case (b), $\mu_a$ of the sample under study varies from 0.04 to 0.3 $cm^{-1}$, while $\mu_s'$ of the sample under study remains 10 $cm^{-1}$. In both cases, the calibration sample has optical properties of $\mu_a = 0.1$ $cm^{-1}$ and $\mu_s' = 10$ $cm^{-1}$.

mean free path of 0.2 cm. The experimental results confirm that when the multiple source–detector separations (3, 5 and 7 cm) are much greater than the optical mean free path (0.2 cm), the spatially resolved, linear approximation, equation (6), for the DC measurement can give rise to correct $\mu_a$ and $\mu_s'$ values, most of which are within 5% errors.

It is known that while the blood changes from deoxygenated to oxygenated state, the extinction coefficient will decrease at 760 nm but increase at 850 nm (Zijlstra *et al* 1991). Based on $\mu_a$ = extinction coefficient × [blood concentration], a decrease/increase in extinction coefficient leads to a decrease/increase in $\mu_a$ if blood concentration remains constant. Consequently, a decrease/increase in $\mu_a$ will result in a decrease/increase in $\mu_{eff}$

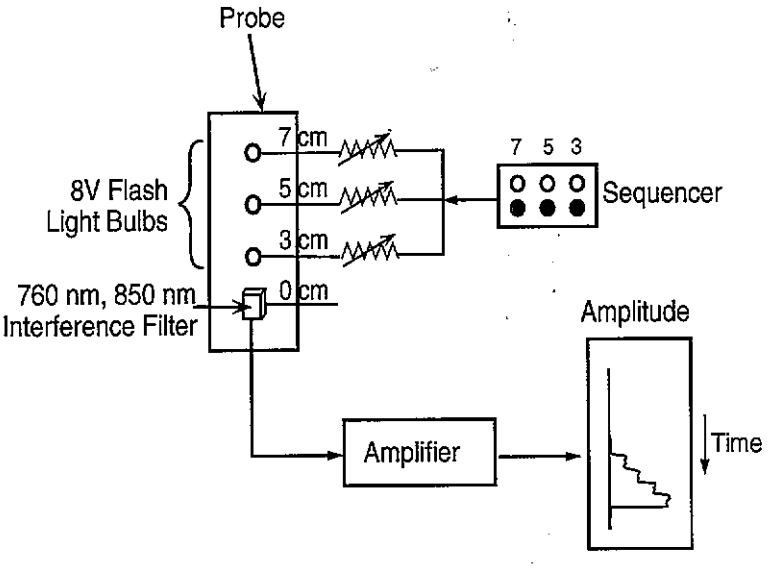


**Figure 4.** Schematic diagram of the electrical circuit for measuring the DC reflectance signal at separations of 3, 5 and 7 cm. Three flashing lightbulbs are mounted on a flexible black tape and turned on in sequence. Their intensities can be tuned by individually adjusting the variable resistors. The detected optical signals are at 760 nm and 850 nm, picked up by using two interference filters, and sent to an amplifier and then to a recorder.

if the scattering property remains unchanged. Figure 6(a) shows changes in $\mu_{\text{eff}}$ of the sample solution during the process of blood oxygenation and deoxygenation at 760 nm and 850 nm. The values of $\mu_{\text{eff}}$ are calculated from the slope of the OD measurements. Figure 6(a) illustrates a correct trend accordingly: $\mu_{\text{eff}}$ values decrease for a 760 nm signal but increase for a 850 nm signal while the blood solution is being oxygenated, and the $\mu_{\text{eff}}$ values at these two wavelengths return to their initial values gradually when the oxygenation process is stopped. Based on equation (5), the ratio of $\mu_{\text{eff}}$ at 760 nm and 850 nm leads to the ratio of $\mu_a$ at these two wavelengths, allowing one to calculate haemoglobin saturation, $Y$. The corresponding saturation values are plotted in figure 6(b), showing an increase and then decrease in haemoglobin saturation during a cycle of the oxygenation process in the blood–yeast model.

In both ink–Intralipid solution and blood–yeast model experiments described above, the variable source–detector separations were chosen to be 3, 5 and 7 cm since the models used were homogeneous and non-high-absorbing materials. However, a smaller range with three or more variable separations can be used, for example, from 2 cm to 3–4 cm, for measuring either high-absorbing or small-dimensional objects. Since the condition for the approximation is $\rho \gg l_t = 1/\mu_t'$, the limit of the nearest separation is set by the optical mean free path. The choice of the range for the variable separations depends mainly on the property and geometry of the tissue sample under study. Also, an increase in number of sources or detectors can improve the accuracy in determining the optical properties.

It is known that all biological tissues contain numerous blood vessels and structural heterogeneity, so it is rare to find perfectly homogeneous tissue for a source–detector separation of 5 or 7 cm. But a recent study (Liu *et al* 1995) showed that the apparent absorption coefficient of a biological organ becomes a volume-weighted sum of the absorption coefficients of blood and background tissue if the diameters of the blood vessels are smaller than a few hundred (~800) micrometres. The same study also demonstrated that

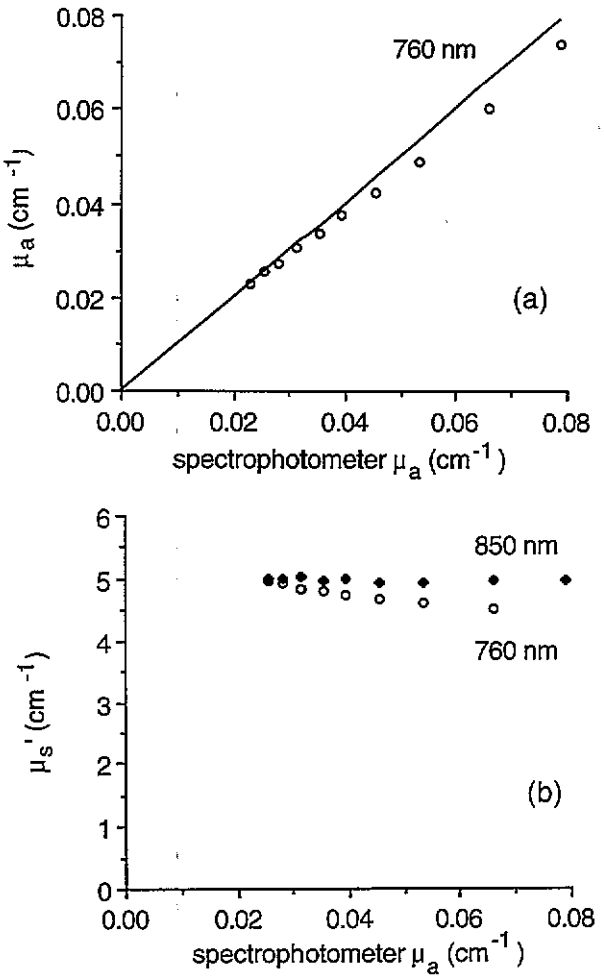


**Figure 5.** (a) Comparison of $\mu_a$ values of ink–Intralipid solution measured with spectrophotometer and with spatial-resolved DC reflectance at 760 nm. The solid line is a unity line. (b) $\mu_s'$ dependence on $\mu_a$ values of the solution at 760 nm and 850 nm. These two figures are calculated based on the slope and intercept of OD versus the separation.

distributed scattering heterogeneities do not affect the absorption determination significantly. This implies that a biological sample can be thought to be homogeneous for absorption measurements if it does not contain many large vessels with ~1 mm diameters or larger. In addition, several theoretical and experimental investigations (Sevick and Chance 1991, Kurth *et al* 1995, Hielscher *et al* 1995) on the head demonstrated that even though the optical properties of the skull are different from the brain, the skull does not have significant influence on the absorption determination of the brain if the source–detector separation is larger than 3 cm. Therefore, as long as a organ has a dimension larger than 2 cm, it is appropriate to apply this spatially resolved, linear-fitting method to obtain optical properties of the sample.

A practical problem of this method to obtain optical properties is how to choose and measure the calibration sample. One may encounter difficulty in keeping the experimental conditions unchanged, while moving the probe from the calibration sample to the unknown

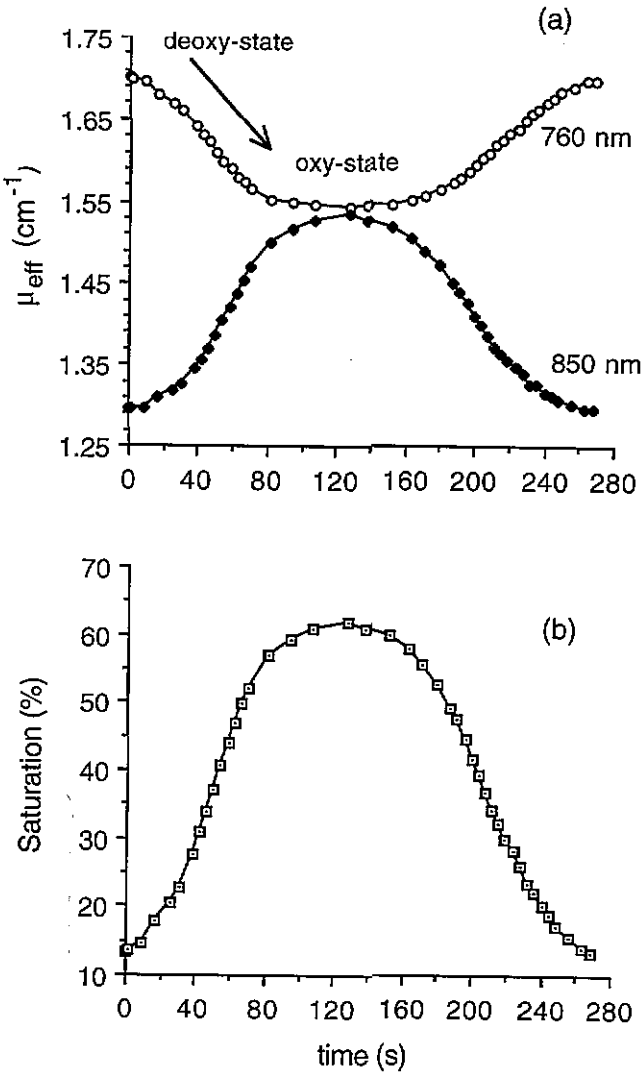


**Figure 6.** (a) Changes in $\mu_{eff}$ of the blood–yeast liquid model measured at 760 nm and 850 nm during a process of deoxy → oxy → deoxy cycle. (b) Corresponding changes in haemoglobin saturation of the liquid model. The calibration sample is the initial deoxygenated blood–yeast model solution.

sample. In our experiments, we always used the initial solution as the calibration sample, avoiding changing any condition between the two samples. Further studies to solve this problem are being undertaken.

In summary, we have introduced a spatially resolved, linear-fitting algorithm to determine the optical properties, $\mu_a$ and $\mu_s'$, and haemoglobin saturation in tissues based on steady-state reflectance data with input–output separations larger than 2 cm, namely 10–20 times the optical mean free path in tissue. By using a calibration sample, one can determine optical density changes with respect to the calibration sample and then calculate

$\mu_a$ and $\mu_s'$ from the slope and intercept. Simulation results show that errors due to the approximation are less than 10% and can be limited by ensuring that the calibration sample has optical properties similar to the sample under study. This indicates that the method is particularly useful for measuring small changes in optical properties of a biological sample. The experimental results of blood–yeast models give correct trends of saturation variation during oxygenating and deoxygenating processes of the model. This demonstrates that with this method, one can use continuous near infrared light to monitor absolute values of haemoglobin saturation in bulk tissue.

## References


Bank W and Chance B 1994 An oxidative defect in metabolic myopathies: diagnosis by noninvasive tissue oximetry *Ann. Neurol.* **36** 830–37

Chance B, Leigh J S, Miyake H, Smith D S, Nioka S, Greenfeld R, Finander M, Kaufmann K, Levy W, Young M, Cohen P, Yoshioka H and Boretsky R 1988a Comparison of time-resolved and -unresolved measurements of deoxyhemoglobin in brain *Proc. Natl Acad. Sci. USA* **85** 4971–5

Chance B, Nioka S, Kent J, McCully K, Fountain M, Greenfeld R and Holtom G 1988b Time-resolved spectroscopy of hemoglobin and myoglobin in resting and ischemic muscle *Anal. Biochem.* **174** 698–707

Cope M and Delpy D T 1988 System for long-term measurement of cerebral blood and tissue oxygenation on newborn infants by near infrared transillumination *Med. Biol. Eng. Comput.* **26** 289–94

Cope M, van der Zee P, Essenpreis M, Arridge S R and Delpy D T 1991 Data analysis method for near infrared spectroscopy of tissue: problems in determining the relative cytochrome aa3 concentration *Proc. Time-Resolved Spectroscopy and Imaging of Tissues, Proc. SPIE-Int. Soc. Opt. Eng.* **1431** 251–62

Delpy D T, Cope M, van der Zee P, Arridge S, Wray Susan and Wyatt J 1988 Estimation of optical pathlength through tissue from direct time of flight measurement *Phys. Med. Biol.* **33** 1433–42

Fantini S, Franceschini-Fantini M A, Maier J S, Walker S A, Barbieri B and Gratton E 1995 Frequency-domain multichannel optical detector for noninvasive tissue spectroscopy and oximetry *Opt. Eng.* **34** 32–42

Farrell T J, Patterson M S and Wilson B 1992a A diffusion theory model of spatially resolved, steady-state diffuse reflectance for the noninvasive determination of tissue optical properties *in vivo Med. Phys.* **19** 879–88

Farrell T J, Wilson B C and Patterson M S 1992b The use of a neural network to determine tissue optical properties from spatially resolved diffuse reflectance measurements *Phys. Med. Biol.* **37** 2281–6

Ferrari M, Wei Q, De Blasi R A, Quaresima V and Zaccanti G 1993 Variability of human brain and muscle optical pathlength in different experimental conditions *Proc. SPIE-Int. Soc. Opt. Eng.* **1888** 466–72

Ferrari M, Zanetti E, Giannini I, Sideri G, Fieschi C and Carpi A 1986 Effects of carotid artery compression test on regional cerebral blood volume, haemoglobin oxygen saturation and cytochrome-c-oxidase redox level in cerebrovascular patients *Adv. Exp. Med. Biol.* **200** 213–22

Flock S T, Jacques S L, Wilson B C, Star W M and van Gemert M J C 1992 Optical properties of Intralipid: a phantom medium for light propagation studies *Lasers Surg. Med.* **12** 510–9

Hielscher A H, Liu H, Chance B, Tittel F K and Jacques S L 1995 Time resolved photon emission from layered turbid media *Appl. Opt.* at press

Jöbsis F F 1977 Noninvasive, infrared monitoring of cerebral and myocardial oxygen sufficiency and circulatory parameters *Science* **19** 1264

Kurth C D, Liu H, Thayer W and Chance B 1995 Dynamic phantom brain model for near infrared spectroscopy *Phys. Med. Biol.* submitted

Liu H, Chance B, Hielscher A H, Jacques S L and Tittel F K 1995 Influence of blood vessels on the measurement of hemoglobin oxygenation as determined by time-resolved reflectance spectroscopy *Med. Phys.* **22** 1209–17

Matcher S J and Cooper C E 1994 Absolute quantification of deoxyhaemoglobin concentration in tissue near infrared spectroscopy *Phys. Med. Biol.* **39** 1–17

Parsa P, Jacques S L and Nishioka N S 1989 Spectral variation of scattering coefficient for rat liver *Appl. Opt.* **28** 2325

Peters V G, Woman D R, Pattern M S and Frank G L 1990 Spectral variation of scattering coefficient for human breast tissue *Phys. Med. Biol.* **35** 1317–34

Sevick E M and Chance B 1991 Photon migration in a model of the head measured using time- and frequency-domain techniques: potentials of spectroscopy and imaging *Proc. Time-Resolved Spectroscopy and Imaging of Tissues, Proc. SPIE-Int. Soc. Opt. Eng.* **1431** 84–96

Sevick E M, Chance B, Leigh J, Nioka S and Maris M 1991 Quantitation of time- and frequency-resolved optical spectra for the determination of tissue oxygenation *Anal. Biochem.* **195** 330–51

Tamura T, Eda H, Takada M and Kubodera T 1990 New instrument for monitoring hemoglobin oxygenation *Adv. Exp. Med. Biol.* **248** 103–7

Thorniley M, Livera L, Wickramasinghe Y, Spenccer S A and Rolfe P 1990 The non invasive monitoring of cerebral tissue oxygenation *Adv. Exp. Med. Biol.* **277** 323

van Staveren H J, Moes C J M, van Marle J, Prahl S A and van Gemert M J C 1991 Light scattering in Intralipid–10% in the wavelength range of 400–1100 nm *Appl. Opt.* **30** 4507–14

Zijlstra W G, Buursma A and Meeuwsen-van der Roest W P 1991 Absorption spectra of human fetal and adult oxyhemoglobin, de-oxyhemoglobin, carboxyhemoglobin, and methemoglobin *Clin. Chem.* **37** 1633–38